2018

Mapping two neurosteroid-modulatory sites in the prototypic pentameric ligand-gated ion channel GLIC

Wayland W. L. Cheng
Washington University School of Medicine in St. Louis

Zi-Wei Chen
Washington University School of Medicine in St. Louis

John R. Bracamontes
Washington University School of Medicine in St. Louis

Melissa M. Budelier
Washington University School of Medicine in St. Louis

Kathiresan Krishnan
Washington University School of Medicine in St. Louis

See next page for additional authors

Follow this and additional works at: https://digitalcommons.wustl.edu/open_access_pubs

Recommended Citation

Authors

Wayland W. L. Cheng, Zi-Wei Chen, John R. Bracamontes, Melissa M. Budelier, Kathiresan Krishnan, Daniel J. Shin, Cunde Wang, Xin Jiang, Douglas F. Covey, Gustav Akk, and Alex S. Evers

Mapping two neurosteroid-modulatory sites in the prototypic pentameric ligand-gated ion channel GLIC

Wayland W. L. Cheng[‡], **Zi-Wei Chen**[‡§], **John R. Bracamontes**[‡], **Melissa M. Budelier**[‡], **Kathiresan Krishnan**[¶], **Daniel J. Shin**[‡], **Cunde Wang**[¶], **Xin Jiang**[¶], **Douglas F. Covey**[‡§‖], **Gustav Akk**[‡§], and **Alex S. Evers**[‡§¶1]

From the Departments of [‡]*Anesthesiology,* [¶]*Developmental Biology, and* [‖]*Psychiatry and the* [§]*Taylor Family Institute for Innovative Psychiatric Research, Washington University, St. Louis, Missouri 63110*

Edited by Henrik G. Dohlman

Neurosteroids are endogenous sterols that potentiate or inhibit pentameric ligand-gated ion channels (pLGICs) and can be effective anesthetics, analgesics, or anti-epileptic drugs. The complex effects of neurosteroids on pLGICs suggest the presence of multiple binding sites in these receptors. Here, using a series of novel neurosteroid-photolabeling reagents combined with top-down and middle-down mass spectrometry, we have determined the stoichiometry, sites, and orientation of binding for 3α,5α-pregnane neurosteroids in the *Gloeobacter* ligand-gated ion channel (GLIC), a prototypic pLGIC. The neurosteroid-based reagents photolabeled two sites per GLIC subunit, both within the transmembrane domain; one site was an intra-subunit site, and the other was located in the interface between subunits. By using reagents with photoreactive groups positioned throughout the neurosteroid backbone, we precisely map the orientation of neurosteroid binding within each site. Amino acid substitutions introduced at either site altered neurosteroid modulation of GLIC channel activity, demonstrating the functional role of both sites. These results provide a detailed molecular model of multisite neurosteroid modulation of GLIC, which may be applicable to other mammalian pLGICs.

Neurosteroids are endogenous brain sterols and allosteric modulators of pentameric ligand-gated ion channels (pLGICs),[2] including GABA_A receptors (GABA_AR) (1), nicotinic acetylcholine receptors (2, 3), and glycine receptors (4, 5). Modulation of these channels is thought to underlie the effect of neurosteroids on neuronal excitability (6, 7) and their pharmacologic potential as anesthetics (8) and treatments for epilepsy (9) and psychiatric disorders (10, 11). Neurosteroids have variable effects on different pLGICs. 3α-Hydroxypregnane neurosteroids potentiate and directly activate the GABA_AR (12), whereas 3β-hydroxysteroids and 3-sulfated neurosteroids inhibit the GABA_AR (13, 14). Certain synthetic neurosteroid analogues both potentiate and inhibit the GABA_AR (15). In addition, neurosteroids can modulate nicotinic acetylcholine receptors (16) and glycine receptors, which may contribute to their potential for the treatment of chronic pain (17). Understanding the structural basis of neurosteroid actions in pLGICs is essential for exploiting their pharmacologic benefits.

Potentiation of the GABA_AR by neurosteroids is thought to occur by binding to the transmembrane domains (TMDs) (18–20). A photoaffinity labeling study identified F301 in the TM3 membrane-spanning domain of the β3 homopentameric GABA_AR as a potential neurosteroid-binding site (21). Recently, crystal structures of a GLIC-GABA_ARα1 chimera and GABA_A Rβ3-α5 chimera identified an equivalent site between TM3 and TM1 of adjacent subunits as a neurosteroid potentiating site (22, 23). However, multiple lines of evidence suggest that potentiation of the GABA_AR by 3α-hydroxypregnane neurosteroids is mediated by more than one site. These include the complex effects of neurosteroids on GABA_AR gating (24), mutations that alter neurosteroid action (25), and radioligand binding (26). Notably, point mutations in the GABA_AR that reduce potentiation or direct activation by 3α-hydroxypregnane neurosteroids localize to disparate regions that have been modeled as two binding sites (25). However, a mutagenesis strategy cannot differentiate between direct effects of mutations on ligand binding and indirect effects on binding or transduction of the ligand signal.

Photoaffinity labeling (PAL) is a more direct approach for identifying ligand-binding sites, where ligands modified to be photoreactive covalently label binding sites. Labeled sites are then identified using mass spectrometry (MS). Although PAL has been an effective approach to identify binding sites of various ligands, including anesthetics (27, 28), identification of neurosteroid-labeled sites has been impeded by the difficulty of recovering and analyzing steroid-modified TMD peptides by MS. These difficulties result from the hydrophobicity of these photolabeled peptides and their tendency to undergo

neutral loss by tandem MS (29, 30). To date, only one neuro-steroid-photolabeled residue in a pLGIC has been reported (21) despite the availability of multiple neurosteroid-photo-labeling reagents (21, 31–33).

Here, we employ an innovative approach that combines a series of 3α-hydroxypregnane neurosteroid-photolabeling reagents with top-down and middle-down MS to determine the stoichiometry, sites, and orientation of neurosteroid binding in a pLGIC. We previously demonstrated the utility of top-down MS to determine the stoichiometry of steroid photolabeling in a membrane protein (29, 30). We now introduce a sensitive and effective middle-down MS strategy, which involves analysis of large TMD peptides for the identification of neurosteroid-pho-tolabeled sites.

In this study, we analyze neurosteroid photolabeling of the bacterial *Gloeobacter* ligand-gated ion channel (GLIC). GLIC is an important structural model of pLGICs (34, 35) and has provided valuable insights on the interaction of allosteric modulators with pLGICs using X-ray crystallography (36–38), molecular modeling (39–42), and PAL (43). GLIC was used in this initial study of pLGICs because 1) it can be readily expressed and purified in milligram quantities, and 2) the absence of glycosylation modifications makes it readily applicable to top-down MS. We demonstrate that GLIC is efficiently labeled by neurosteroid-photolabeling reagents with a stoichiometry of two per subunit and delineate distinct intersubunit and intrasubunit binding pockets. By using complementary photoreactive moieties positioned throughout the neurosteroid backbone, we map the preferred orientation of neurosteroids within these sites. Mutational analysis demonstrates that both photolabeled sites mediate neurosteroid inhibition of GLIC channel activity. The findings of this study provide a structural model for multisite neurosteroid modulation of the prototypic pLGIC, GLIC, which may be applicable to mammalian pLGICs.

Results

Neurosteroids photolabel the TMD of GLIC with a stoichiometry of two

To determine the stoichiometry of neurosteroid binding in a pLGIC, we photolabeled purified *n*-dodecyl-β-D-maltoside (DDM)-solubilized GLIC with (3α,5α)-6-azi-pregnanolone (5α-6-AziP) (Fig. 1*A*), a photoreactive analogue of the endogenous neurosteroid allopregnanolone, and analyzed the labeled protein using top-down MS. MS analysis of intact photolabeled GLIC demonstrates efficient labeling by 5α-6-AziP at 100 μM (Fig. 1*C*; Table S1) and at 100 μM labeled three times, with a labeling stoichiometry of two (*i.e.* two neurosteroids per GLIC subunit) (Fig. 1, *B* and *D*). Top-down fragmentation by higher-energy collisional dissociation (HCD) of the singly labeled GLIC species yields a series of 5α-6-AziP-containing y-ions that localize at least one of the labeled sites to the C-terminal end of TM3 or TM4 (Fig. 1*E*). Although analysis of intact GLIC clearly demonstrates the stoichiometry of labeling, top-down fragmentation yields poor sequence coverage of the GLIC protein and thus inadequate localization of the labeled sites.

To further localize 5α-6-AziP labeling, we applied a middle-down MS strategy by digesting GLIC with specific endoproteinases. Digestion of GLIC by AspN, an endoproteinase that cleaves at the N-terminal end of aspartate residues (44), predominantly cleaves at an aspartate between the extracellular domain (ECD) and TMD leaving each domain intact (Table S1). MS analysis of the ECD and TMD of GLIC labeled with 5α-6-AziP reveals no detectable labeling in the ECD and efficient labeling of the TMD with a stoichiometry of two (Fig. 2, *A* and *B*). HCD fragmentation of the singly labeled TMD species yields extensive sequence coverage with 5α-6-AziP-containing b- and y-ions that identify two photolabeled sites located in the N-terminal end of TM1 and the C-terminal end of TM3, respectively (Fig. 2*C*). Thus, systematic top-down and middle-down MS analyses of GLIC reveal a labeling stoichiometry of two within the TMD.

Identification of two neurosteroid-photolabeled sites in the GLIC TMD

To identify the residues labeled by 5α-6-AziP in the GLIC TMD, we applied a middle-down MS analysis using trypsin. Trypsin digestion of DDM-solubilized GLIC yields three large peptides composed of transmembrane helix 1 and 2 (TM1 + 2), TM3, and TM4. We find that keeping these TMD peptides in DDM for LC-MS analysis is an effective method for maintaining the solubility and stability of neurosteroid-labeled peptides. In addition, because of the large size of these peptides, neurosteroid-labeled peptides show minimal neutral loss by collision-induced dissociation (CID) or HCD fragmentation, facilitating localization of the labeled residues. Tryptic digests of GLIC photolabeled with 100 μM 5α-6-AziP show labeling of all three TMD peptides with efficiencies of 5% for TM1 + 2, 32% for TM3, and 1.0% for TM4 (Fig. 3*A*). As expected, the more hydrophobic 5α-6-AziP-labeled peptides are shifted to higher retention times with reverse-phase LC-MS.

CID or HCD fragmentation spectra for these three 5α-6-AziP-labeled TMD peptides show that 5α-6-AziP labels Glu-272 in TM3 (Fig. 3*B*); labeling was localized to one of three adjacent residues (Gln-193–Phe-195) in TM1 (Fig. 3*C*) and one of three adjacent residues (Phe-315–Phe-317) at the C terminus of TM4 (Fig. 3*D*). Examination of these labeled residues in the GLIC crystal structure (45) reveals two distinct foci of labeling as follows: one formed by the C-terminal end of TM3 (Glu-272) and another between the N-terminal end of TM1 (Tyr-194) and the C-terminal end of TM4 (Phe-315; Gly-316 and Phe-317 are not resolved in the GLIC crystal structure) (Fig. 3*E*). Glu-272 in TM3 is near an intersubunit neurosteroid-binding site previously defined by photolabeling in the β3 homopentameric GABA$_A$R (21) and GABA$_A$R chimera crystal structures with bound 3α,5α-tetrahydrodeoxycorticosterone (THDOC) and pregnanolone neurosteroids (22, 23). Because 5α-6-AziP is an aliphatic diazirine that may preferentially label nucleophilic side chains such as glutamate (28, 29), we tested labeling of the E272A GLIC mutant. The DDM-solubilized E272A mutant was purified as a pentamer and is also labeled by 5α-6-AziP with a stoichiometry of two (Fig. 4*A*; Table S1). As in WT, E272A is labeled by 5α-6-AziP at the C-terminal end of TM1 and TM4 (Fig. 4, *C* and *D*), but, in contrast to WT, E272A
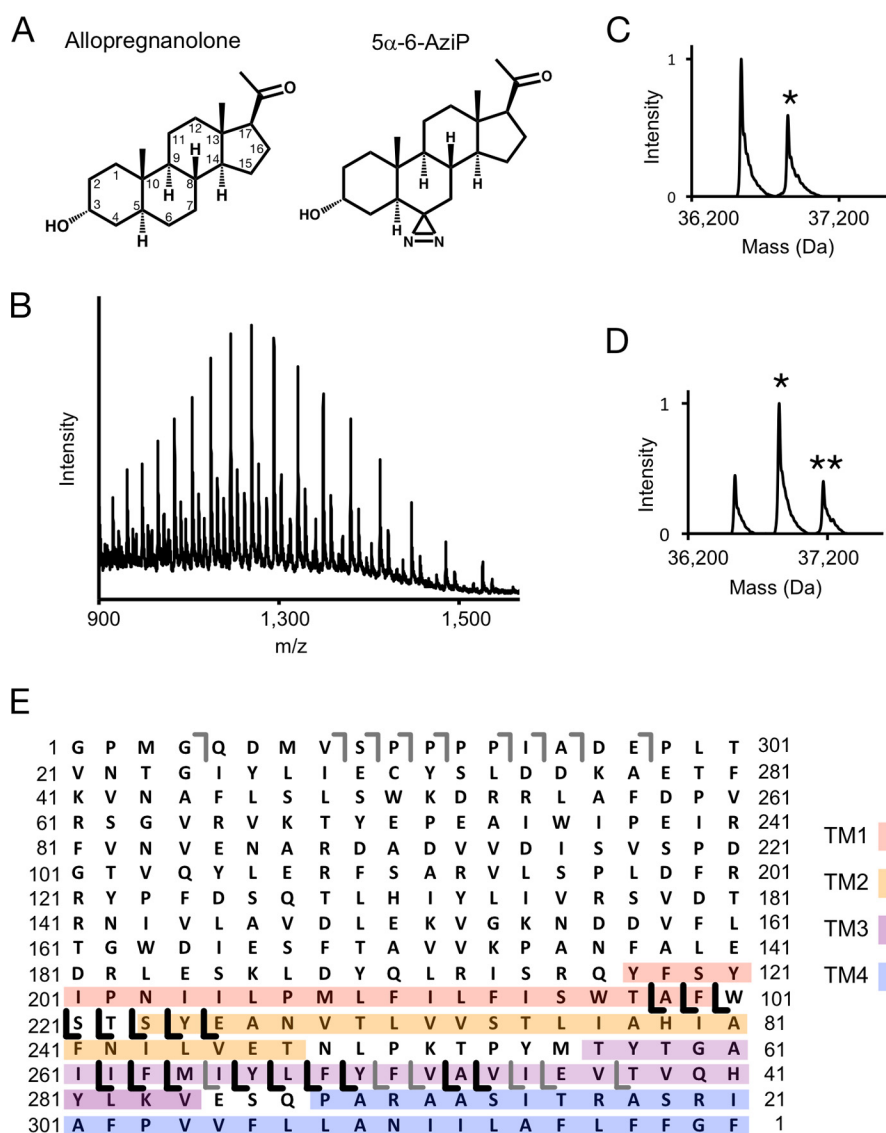
Figure 1. Top-down analysis of GLIC photolabeled with 5α-6-AziP. *A,* structure of allopregnanolone and 5α-6-AziP. Asterisks denote the number of 5α-6-AziP labels. *B,* full spectrum of GLIC labeled with 100 μM 5α-6-AziP three times, acquired on an Elite LTQ. *C,* deconvoluted spectrum of GLIC photolabeled with 100 μM 5α-6-AziP. *Asterisks* denote the number of 5α-6-AziP labels per GLIC subunit. *D,* deconvoluted spectrum of GLIC photolabeled with 100 μM 5α-6-AziP three times. *E,* fragment ions from top-down HCD of the 32+ charge state of singly labeled GLIC from the spectrum in *B.* The *gray* b- and y-ions are fragment ions that contain no 5α-6-AziP, and the *black* y-ions contain 5α-6-AziP. The TMDs are color-coded.

is labeled at Tyr-278 in TM3 (Fig. 4B), which supports neurosteroid binding to an intersubunit site between TM3 and TM1 of adjacent subunits (Fig. 3E). Although the exact labeled residue was not identified in TM1, we favor labeling of Tyr-194 because the side chain points toward an intrasubunit site encompassed by the C terminus of TM4, and Tyr-194 is the only nucleophile in the Gln-193–Tyr-194–Phe-195 segment where 5α-6-AziP labels. Docking simulations were performed for allopregnanolone in the TMD region of a GLIC pentamer, revealing a dominant cluster of poses located in an intersubunit site adjacent to Glu-272 and Tyr-278 (Fig. 3E). To search for additional sites, a second allopregnanolone molecule was docked to the GLIC TMD with one allopregnanolone molecule placed within the intersubunit site. This yielded additional binding clusters, including one located in an intrasubunit site encompassed by Tyr-194 and Phe-315 (Fig. 3E). Thus, our photolabeling results reveal two putative neurosteroid-binding sites: an intersubunit

site between TM3 and TM1 of adjacent subunits and an intrasubunit site between TM1 and TM4.

Mapping the orientation of neurosteroid binding within both sites

The structure of neurosteroids, particularly at the 3- and 5-positions of the steroid backbone, are critical determinants of modulation of pLGICs (4, 46, 47), suggesting that neurosteroids bind to sites in these channels with a particular orientation. To map the orientation of neurosteroid binding in GLIC, we synthesized 5α-12-AziP and 5α-15-AziP where the photoreactive diazirine is placed in the 12- and 15-positions of the steroid backbone, respectively (Fig. 5A). Analysis of GLIC labeled with 100 μM 5α-6-AziP, 5α-12-AziP, or 5α-15-AziP shows significantly higher photolabeling efficiency for 5α-6-AziP compared with 5α-12-AziP or 5α-15-AziP for TM3 and TM1 + 2 (Fig. 5B). In contrast, non-specific labeling of the peptide YGGFLRF
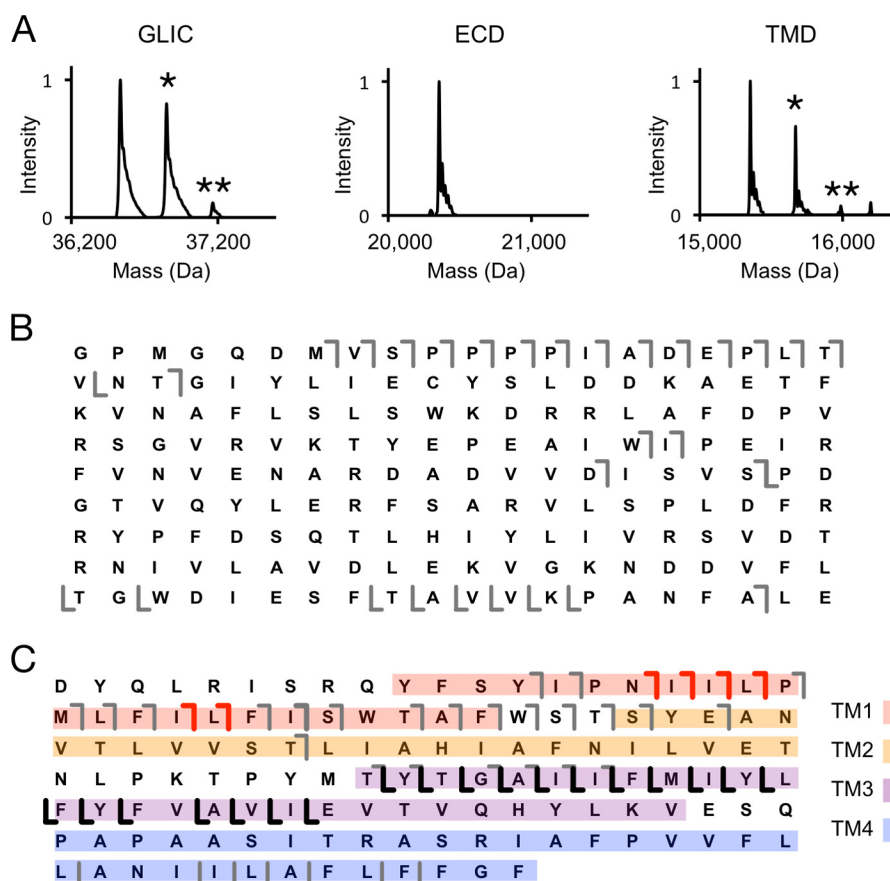
Figure 2. AspN middle-down analysis of GLIC photolabeled with 5α-6-AziP. *A,* deconvoluted spectra of GLIC photolabeled with 300 μM 5α-6-AziP showing intact GLIC and the ECD and TMD after AspN digestion. *B,* HCD fragment ion assignments of the unlabeled ECD peptide shown in *A.* The *gray lines* represent b- and y-ions that do not contain 5α-6-AziP. *C,* HCD fragment ion assignments of the singly labeled TMD species in *A.* The *red* and *black lines* represent b-ions and y-ions, respectively, that contain 5α-6-AziP.

by these reagents shows similar labeling efficiencies, indicating that they are equally photoreactive (Fig. 5B). 5α-12-AziP and 5α-15-AziP both label TM3 at Glu-272 (Fig. 5, *C* and *D*), and no detectable labeling of TM1 + 2 was observed for these reagents. To explore potential binding poses, allopregnanolone was docked to the intersubunit and intrasubunit sites, which revealed poses where the neurosteroid has opposite orientations with respect to the 3- and 17-positions (Fig. 6). For the intersubunit site, approximately equal numbers of poses were obtained with allopregnanolone in either orientation (Fig. 6A), whereas the intrasubunit site showed a predominant docking orientation with the 3-hydroxy pointing extracellularly (Fig. 6B). The higher labeling efficiency for 5α-6-AziP compared with 5α-12-AziP or 5α-15-AziP indicates that the 6-position of the neurosteroid is most proximal to Glu-272 in TM3 and Tyr-194 in TM1. Thus, the photolabeling data are consistent with a neurosteroid binding orientation where the 3-hydroxy is pointing intracellularly for the intersubunit site and extracellularly for the intrasubunit site (Fig. 7, *A* and *B*). Although the equal number of allopregnanolone docking poses obtained for each orientation at the intersubunit site does not suggest a preferred orientation, we believe that photolabeling data provide better discrimination of orientation than docking to a static crystal structure. Careful inspection of allopregnanolone docking poses in both sites shows the nature of the interactions for these preferred binding modes (Fig. 6). For the intersubunit site, allo-

pregnanolone forms closer van der Waals interactions with Trp-317 when the 3-hydroxy points intracellularly; the 3-hydroxy may also form a hydrogen bond interaction with the Tyr-278 aromatic ring. For the intrasubunit site, the preferred orientation results in hydrogen bonds between the 3-hydroxy of allopregnanolone and backbone carbonyl of Phe-121, and between the 20-carbonyl of allopregnanolone and Tyr-254 hydroxyl. In contrast, one weak hydrogen bond is present between the 20-carbonyl of allopregnanolone and Tyr-194 hydroxyl when allopregnanolone is in the opposite orientation. 5α-6-AziP, 5α-12-AziP, and 5α-15-AziP were also docked to GLIC at both sites. In each case, among the most populated binding clusters are poses with the 6-diazirine closest to Glu-272 for the intersubunit site and Tyr-194 for the intrasubunit site (Fig. 7).

Given the inherent preference of 5α-6-AziP, 5α-12-AziP, and 5α-15-AziP for nucleophilic residues, we synthesized two additional neurosteroid-photolabeling reagents, KK200 and CW12 (Fig. 8, *A* and *B,* supporting Material) (33), which contain a trifluoromethylphenyl-diazirine (TPD) group in the 17- and 11-positions, respectively, and are expected to not show the same preference for nucleophiles as aliphatic diazirines (28, 49). Similar to 5α-6-AziP, 100 μM KK200 efficiently labels GLIC (22% efficiency) and shows a labeling stoichiometry of two (Fig. 8A). In contrast, CW12 labels GLIC with low efficiency (<1%) (Fig. 8B). Tryptic analysis of
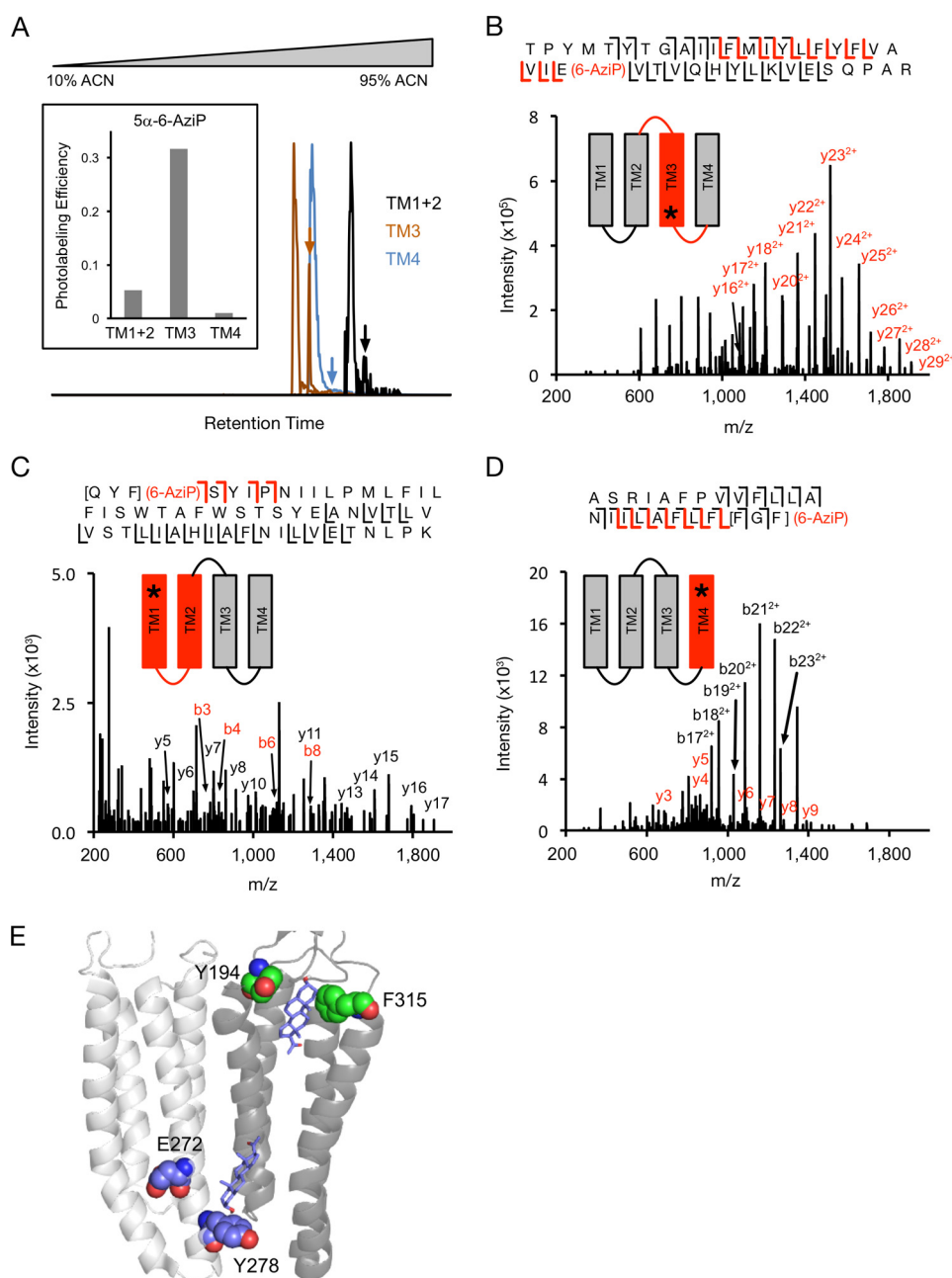
Figure 3. Trypsin middle-down analysis of GLIC photolabeled with 5α-6-AziP. *A,* extracted chromatograms of unlabeled and 5α-6-AziP-labeled (denoted by *arrows*) TM1 + 2, TM3, and TM4 peptides, normalized to the intensity of each unlabeled peptide. *Inset graph* shows the labeling efficiency of each peptide. *B,* HCD MS2 spectrum of TM3 labeled with 5α-6-AziP where (*6-AziP*) indicates labeling of the residue(s) to the *left*. *Red* and *black* fragment ions do and do not contain 5α-6-AziP, respectively. The schematic shows in *red* the TMD being analyzed, and the *asterisk* denotes the approximate location of 5α-6-AziP. *C,* HCD MS2 spectrum of TM1 + 2 labeled with 5α-6-AziP from GLIC. *D,* CID MS2 of TM4 labeled with 5α-6-AziP from GLIC. The b_{22}^{+} and b_{23}^{+} represent neutral loss of adduct. *E,* GLIC structure (PDB 4HFI) highlighting the photolabeled residues in the intersubunit (*purple spheres*) and intrasubunit sites (*green spheres*) and docking poses for allopregnanolone (*purple sticks*) at both sites.

GLIC labeled with KK200 shows labeling of TM3 and TM4 peptides (efficiencies of 7 and 29%, respectively), and fragmentation spectra localize KK200 labeling to Phe-267 in TM3 (Fig. 8C) and Asn-307 in TM4 (Fig. 8D). Phe-267 is located near the intersubunit-binding site, and labeling of this residue by KK200 is consistent with the orientation proposed above for allopregnanolone, where the neurosteroid lies in the interface between TM3 of one subunit and TM1 of the adjacent subunit with the 17-position pointing toward the extracellular surface (Fig. 6A). Asn-307 is located near the intrasubunit site, and labeling of this residue by KK200 is consistent with an orientation where the 17-position points toward the intracellular surface (Fig. 6B). No KK200 photolabeling was identified in the ECD using a PEAKS search (97% sequence coverage), confirming that the TPD group does not point extracellularly and labels the ECD from within the intrasubunit site. Docking of KK200 to both sites reveals binding poses in agreement with these findings where the diazirine lies adjacent to Phe-267 and Asn-307 (Fig. 7). Docking poses of CW12 to both sites suggest that the 11-TPD group is likely
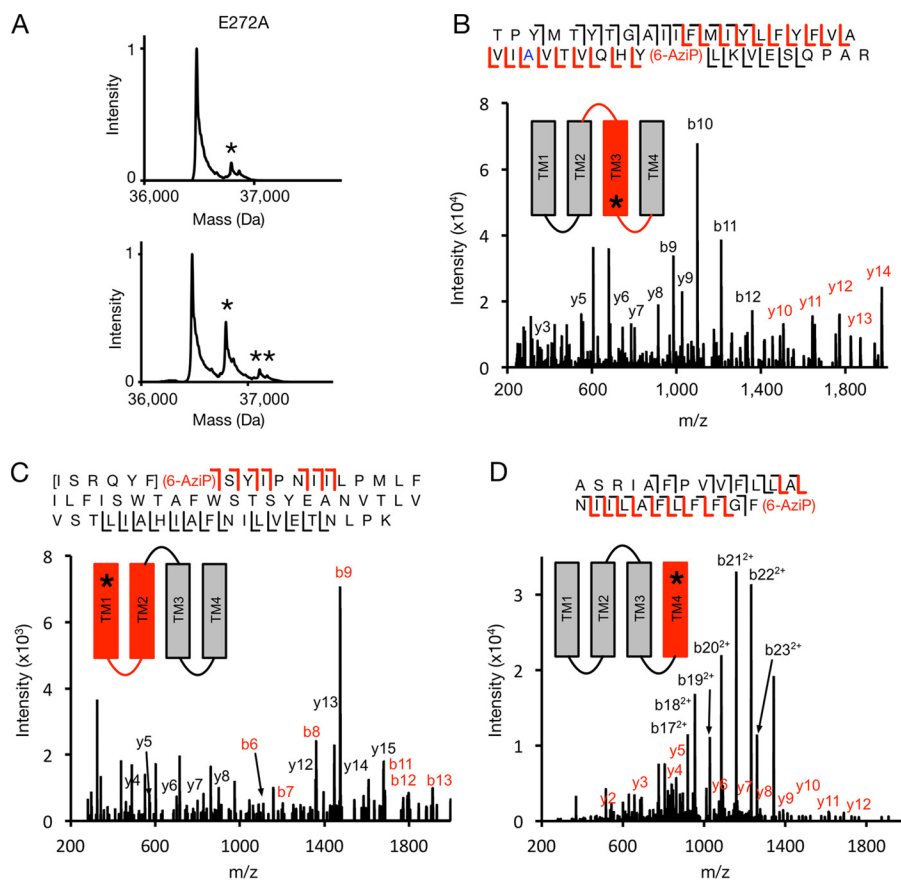
Figure 4. MS analysis of E272A GLIC photolabeled with 5α-6-AziP. *A,* deconvoluted spectra of GLIC E272A labeled with 100 μM 5α-6-AziP (*left*) or 100 μM three times (*right*). The *asterisks* denote GLIC E272A labeled with one or two 5α-6-AziP. *B,* CID MS2 spectrum of TM3 labeled with 5α-6-AziP from E272A GLIC. *Red* and *black* b- and y- ions do and do not contain 5α-6-AziP, respectively. Schematic highlights in *red* the TMD being analyzed, and the *asterisk* denotes the approximate location of 5α-6-AziP. *C,* HCD MS2 spectrum of TM1 + 2 peptide from GLIC E272A labeled with 5α-6-AziP. *D,* CID MS2 spectrum of TM4 peptide labeled with 5α-6-AziP from GLIC E272A.

pointing away from GLIC toward the lipid bilayer, consistent with the low labeling efficiency of CW12 in GLIC (Fig. 7).

Using a series of neurosteroid-photolabeling reagents, we have precisely mapped two neurosteroid-photolabeled sites in GLIC. To confirm that neurosteroids bind to these photolabeled sites, we tested the ability of neurosteroids to competitively prevent labeling. We examined the labeling efficiency of TM3 by 10 μM 5α-6-AziP (intersubunit site) and TM4 by 10 μM KK200 (intrasubunit site) in the absence and presence of 100 μM allopregnanolone and CW12. 5α-6-AziP labeling of TM3 and KK200 labeling of TM4 were examined because these gave the highest labeling efficiencies at 10 μM. For 5α-6-AziP labeling of TM3, allopregnanolone and CW12 significantly reduce the labeling efficiency (Fig. 9A). KK200 labeling of TM4 is significantly reduced by CW12, whereas allopregnanolone causes a reduction of labeling that is not statistically significant (Fig. 9B). Thus, a neurosteroid analogue, CW12, prevents labeling at both sites. Prevention of KK200 labeling at the intrasubunit site by allopregnanolone is not statistically significant possibly because it has a lower affinity for this site compared with KK200. Indeed, we have found that competition of photolabeling by neurosteroid-based reagents is often difficult to demonstrate, and we suspect that this is due to the fact that labeling is an irreversible process and neurosteroids bind with relatively low affinity

(21, 27, 29). CW12 prevention of labeling at both sites supports the interpretation that the low labeling efficiency of this reagent is due to the position of the TPD photolabeling moiety in the steroid backbone and not an inability of this reagent to bind to these sites.

Both neurosteroid-binding sites mediate modulation of GLIC activity

We next examined the functional effect of allopregnanolone on GLIC channel activity using two-electrode voltage clamp recordings of *Xenopus* oocytes. At pH50 for activation, 30 μM allopregnanolone as well as the photolabeling reagents 5α-6-AziP, 5α-12-AziP, 5α-15-AziP, KK200, and CW12 significantly inhibit GLIC activity ranging from 8 to 86% inhibition (Fig. 10; Tables 1 and 2). To determine the functional involvement of the intersubunit- and intrasubunit-photolabeled sites in mediating the inhibitory effect of neurosteroids, we mutated residues within both binding pockets as predicted by the allopregnanolone-docking model (Fig. 11A). In the intersubunit site, we generated I271W, W213A, and W217A; however, only I271W produced functional receptors. I271W is predicted to introduce significant steric hindrance to the intersubunit site. In the intrasubunit site, we generated F121A and Y254A. F121A is predicted to remove key van der Waals interactions with the neurosteroid
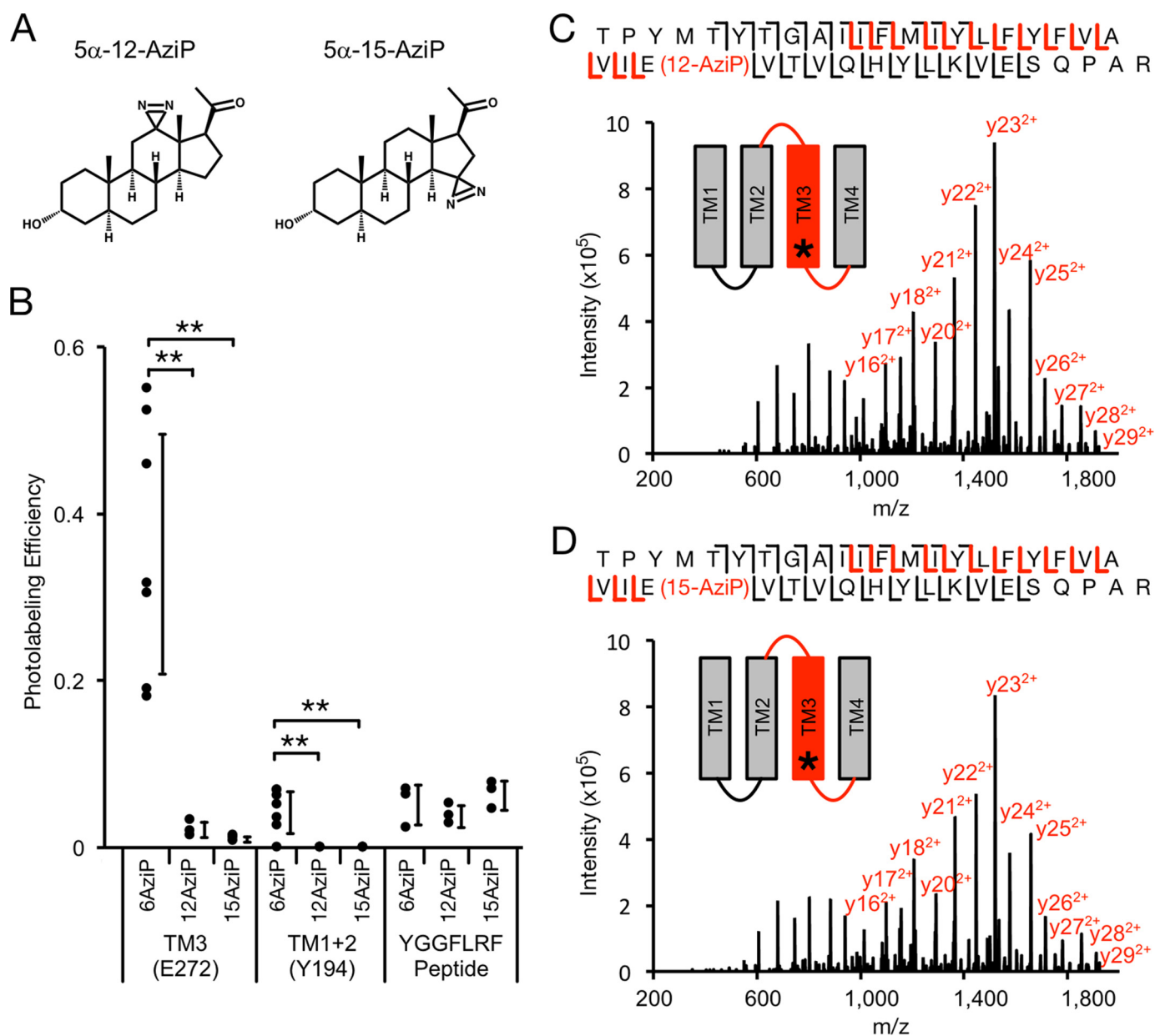
Figure 5. MS analysis of GLIC photolabeled with 5α-12-AziP and 5α-15-AziP. *A*, structure of the photolabeling reagents 5α-12-AziP and 5α-15-AziP. *B*, photolabeling efficiency of 5α-6-AziP, 5α-12-AziP, and 5α-15-AziP for TM3 and TM1 + 2 of WT GLIC, and the peptide YGGFLRF ($n = 7$ for 5α-6-AziP, $n = 3$ for 5α-12-AziP and 5α-15-AziP). ±S.D., **, $p < 0.01$. *C*, HCD MS2 spectrum of TM3 peptide labeled with 5α-12-AziP from GLIC WT. *Red* and *black* fragment ions do and do not contain 5α-12-AziP, respectively. *D*, same as *C* for 5α-15-AziP.

ring structure, and Y254A is predicted to remove a hydrogen bond interaction between Tyr-254 and the neurosteroid 20-carbonyl. Inhibition by 5α-6-AziP was abolished in F121A (resulting in potentiation) and Y254A but not I271W (Fig. 11, *B and C*; Table 2). In contrast, inhibition by KK200, which was the strongest inhibitor of all neurosteroid analogues tested, was abolished in F121A and significantly reduced in I271W and Y254A (Fig. 11, *B and C*; Table 2). Inhibition by allopregnanolone was abolished in F121A and Y254A (resulting in potentiation) but was unaffected by I271W (Fig. 11*C*; Table 2). Thus, the results obtained with KK200 support the hypothesis that binding of certain neurosteroid analogues to either the intersubunit or intrasubunit site results in allosteric inhibition of GLIC activity. There is a loss of inhibition in F121A and Y254A but no

significant effect in I271W for 5α-6-AziP or allopregnanolone suggesting that binding of these compounds to the intrasubunit site predominantly mediates their inhibitory effect. To distinguish whether the increased inward current evoked by 5α-6-AziP (and allopregnanolone) in F121A channels represents potentiation of low pH activation or direct activation, we examined the effect of 30 μM 5α-6-AziP on the holding current at pH 7.6 ($n = 5$). The absence of any effect on the holding current suggests that 5α-6-AziP potentiates the effect of low pH rather than directly activating the channel. To test whether potentiation of F121A by allopregnanolone and 5α-6-AziP is due to unmasking of a potentiating intersubunit site, we generated the F121A/I271W double mutant, but we found that this construct does not express currents in oocytes.
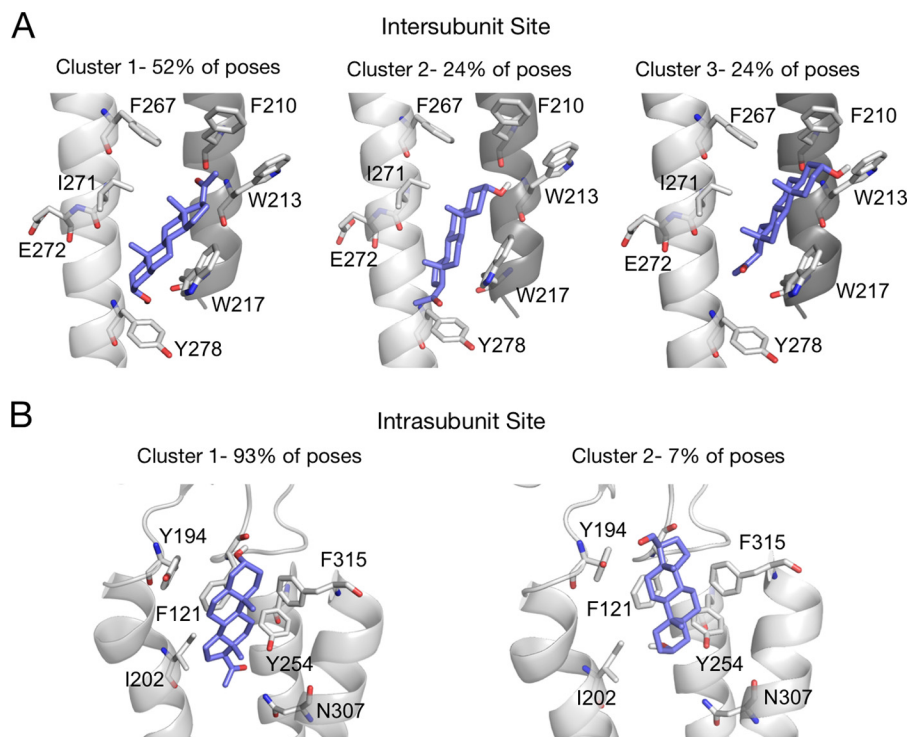
Figure 6. 5α-6-AziP-photolabeled residues are consistent with docking poses within an intersubunit- and intrasubunit-binding site. *A,* clusters of poses for allopregnanolone docked within the intersubunit site indicating the percent of total poses represented by each cluster. Cluster 1 is most consistent with the preferred binding orientation from the photolabeling data. *B,* same as *A* for the intrasubunit site. Cluster 1 is most consistent with the preferred binding orientation from the photolabeling data. Cluster 1 shows hydrogen bond interactions between the neurosteroid 3-hydroxy and backbone carbonyl of Phe-121 (distance of 2.3 Å), and the neurosteroid 20-carbonyl and Tyr-254 hydroxyl (distance of 2.0 Å). Cluster 2 shows a weak hydrogen bond between the neurosteroid 20-carbonyl and the Tyr-194 hydroxyl (distance of 4.0 Å). *B,* same as *A* for the intersubunit site.

Discussion

Neurosteroids are potent endogenous molecules that modulate the activity of neuronal pLGICs and are being developed as anti-epileptics, anti-depressants, general anesthetics, analgesics for chronic pain, and neuroprotective agents (7). This study demonstrates precise mapping of two neurosteroid-binding sites in a prototypic pLGIC, GLIC, using a series of novel neurosteroid-photolabeling reagents. Confident identification of the stoichiometry and sites of labeling was enabled by analysis with top-down and middle-down MS approaches. Two recent studies report crystal structures of a GLIC-GABA$_A$Rα1 chimera and GABA$_A$Rβ3-α5 chimera with a single-bound THDOC and pregnanolone, respectively, at the same intersubunit site identified by our photolabeling reagents (22, 23). In contrast, we report a second functionally relevant 3α-hydroxypregnane neurosteroid-binding site in the pLGIC GLIC. We think that this discrepancy is due the challenge of obtaining crystallized structures of membrane proteins complexed with steroids, and we anticipate that the photolabeling approach introduced in this study will enable sensitive identification of neurosteroid-binding sites in other integral membrane proteins. Of note, the intrasubunit site identified in this study for allopregnanolone is distinct from an intrasubunit site identified for the inhibitory neurosteroid, pregnenolone sulfate, in a GLIC-GABA$_A$Rα1 chimera crystal structure between the intracellular end of TM3 and TM4 (22).

Identification of two neurosteroid-binding sites that modulate GLIC activity is consistent with the complex effects of neurosteroids in the GABA$_A$R and glycine receptor, which suggest

that multiple binding sites also exist in these receptors (4, 24, 50). The intersubunit and intrasubunit sites identified in this study may be neurosteroid-binding pockets shared among pLGICs and thus provide a structural framework for understanding neurosteroid interactions with pLGICs in general. The presence of the intersubunit neurosteroid site in GLIC is consistent with the finding that the Q241L mutation in the GABA$_A$R α1 subunit abolishes neurosteroid potentiation (25). This site was previously identified by the neurosteroid-photolabeling reagent 5β-6-azi-pregnanolone in the β3 homopentameric GABA$_A$R (21) and recently by neurosteroid-bound GABA$_A$R chimera crystal structures (22, 23). In the GABA$_A$R, the neurosteroid 3-hydroxy forms a hydrogen bond with Gln-241 in TM1, which is the opposite orientation than we determined for neurosteroid binding in this site in GLIC. We propose that the preferred orientation of neurosteroids within these sites will vary for different pLGICs depending on the exact molecular composition of the sites, and that key interactions with the protein will determine transduction of neurosteroid binding to effect potentiation or inhibition. For example, although allopregnanolone, 5α-6-AziP, and KK200 all bind to the intersubunit site in GLIC, only KK200 inhibition is reduced by the I271W mutation suggesting that interaction of the KK200 TPD group within this site results in an inhibitory effect.

The presence of an intrasubunit neurosteroid site at the extracellular end of TM1 and TM4 in GLIC is also consistent with prior mutagenesis studies in other pLGICs. Mutations of Asn-407 and Tyr-410 in TM4 of the GABA$_A$R α1 subunit
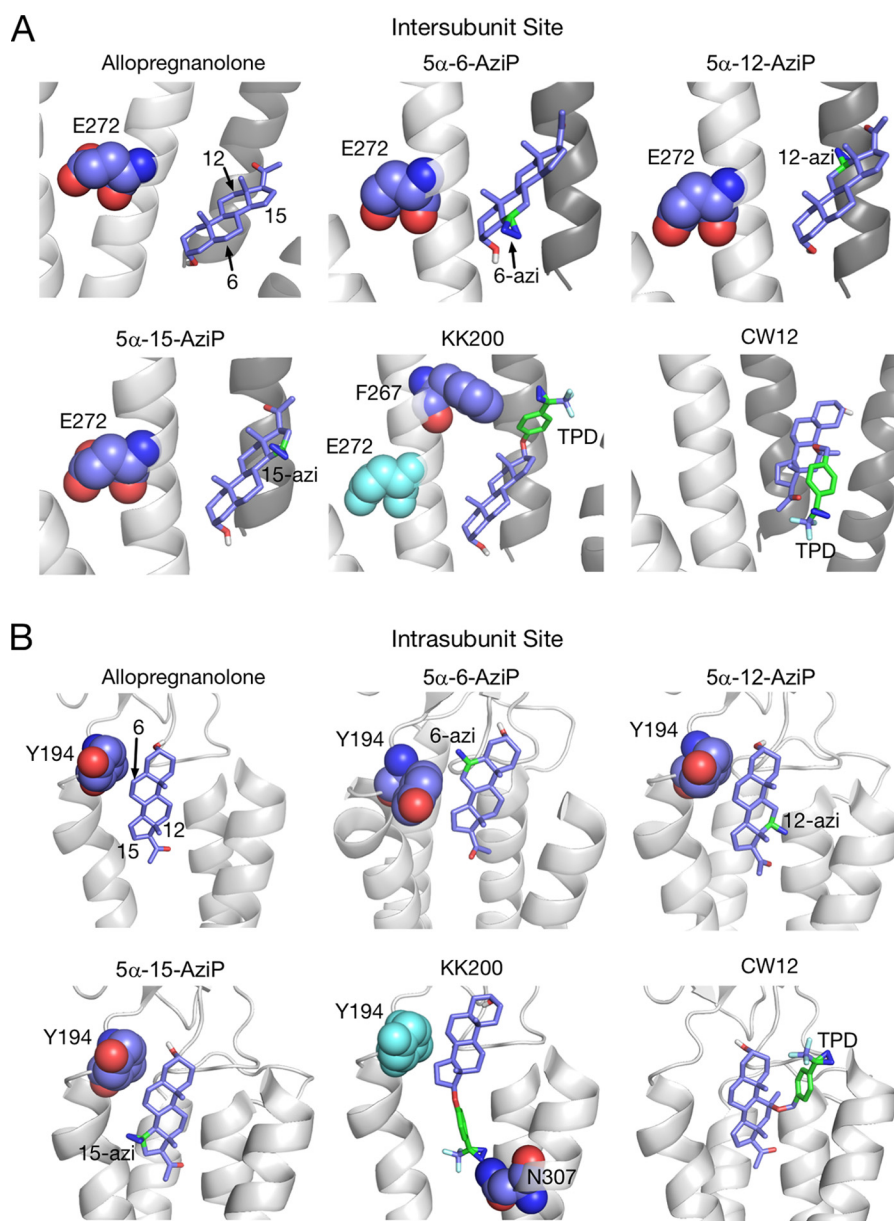
Figure 7. Docking poses of allopregnanolone and photolabeling reagents in the intersubunit and intrasubunit sites. *A,* binding poses selected from among the three most populated clusters for allopregnanolone, 5α-6-AziP, 5α-12-AziP, 5α-15-AziP, KK200, and CW12 in the intersubunit site. The photolabeled residues, Glu-272 (*5α-6-AziP, 5α-12-AziP, 5α-15-AziP*) and Phe-267 (*KK200*), are shown as *purple spheres*. The positions of the allopregnanolone steroid backbone or the photo-labeling groups are labeled. *B,* same as *A* for the intrasubunit site where the photolabeled residue, Tyr-194 (*5α-6-AziP*) and Asn-307 (*KK200*), are shown as *purple spheres*.

reduce neurosteroid potentiation (25), and mutation of the C terminus of the GABA$_A$R γ2 subunit (24) or nicotinic acetyl-choline receptor α4 subunit (51) reduce potentiation of these pLGICs by neurosteroids or an estrogenic steroid, respectively. The intrasubunit neurosteroid site is located at the extracellular end of TM1 and TM4 and, in GLIC, is also composed of Phe-121 from the β6-β7 loop in the ECD. The F121A mutant reduces inhibition by all tested neurosteroid analogues, allo-pregnanolone, 5α-6-AziP, and KK200, which is consistent with our model that shows this residue forming close van der Waals interactions with the neurosteroid ring structure. Contribution of an ECD loop to a neurosteroid-binding site is novel to our current understanding of neurosteroid interactions with pLGICs, and it has implications for understanding neuros-teroid modulation of prokaryotic ECD/eukaryotic TMD pLGIC

chimeras. For example, a recently characterized GLIC-GABAρ1 chimera recapitulates neurosteroid stereoselectivity at the 5-position characteristic of ρ1 receptors. However, although ρ1 receptors are potentiated by 5α-THDOC, the chimera and GLIC are both inhibited by 5α-THDOC (52). This was attrib-uted to the impact of ECD–TMD coupling interactions that affect gating, but it may also result from an ECD contribution to a neurosteroid-binding site. Indeed, we find that the direction-ality of the neurosteroid effect is determined, in part, by the structure of the intrasubunit-binding site, because the F121A mutant reverses the effect of 5α-6-AziP and allopregnanolone from inhibition to potentiation. An alternative explanation to this finding is that the F121A mutation unmasks the effect of a neurosteroid potentiating site for 5α-6-AziP and allopregnano-lone, which may be the intersubunit site. It is also intriguing
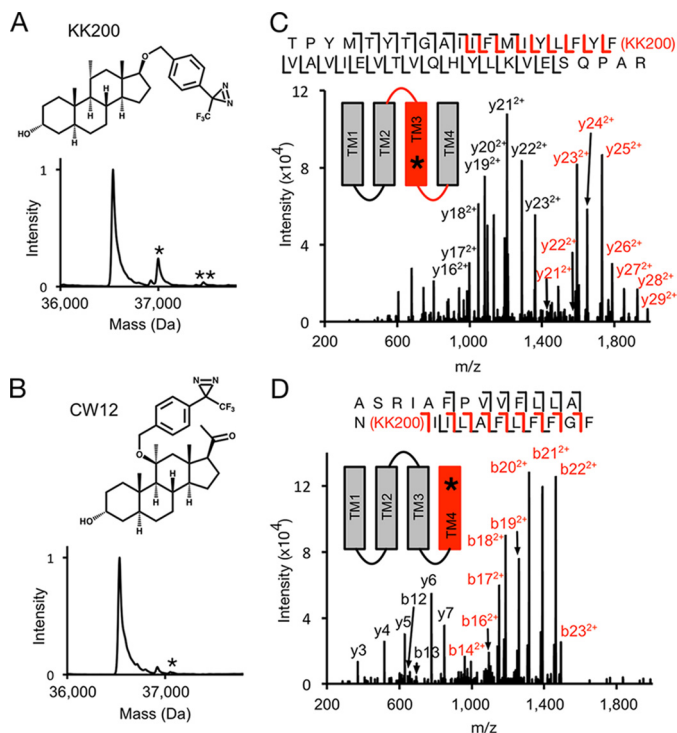
Figure 8. MS analysis of GLIC photolabeled with KK200 and CW12. *A,* structures and deconvoluted spectra of intact GLIC photolabeled with 100 μM KK200. *Asterisk* denotes number of photolabels. *B,* same as *A* for CW12. *C,* CID MS2 spectrum of TM3 labeled with KK200 from GLIC. The unlabeled y_{21}^+, y_{22}^+, and y_{23}^+ ions represent neutral loss of adduct. *Red* and *black* fragment ions do and do not contain KK200, respectively. *D,* HCD MS2 spectrum of TM4 labeled with KK200 from GLIC.

that mutations at either the intersubunit or intrasubunit site nearly abolish KK200 inhibition of GLIC. This indicates that, in the case of KK200, both sites are necessary for inhibition and suggests that there is either a cooperative interaction between these sites or that mutations at one site affect the other.

Two neurosteroid-binding sites in GLIC raise the question as to whether these sites, particularly the intrasubunit site, mediate potentiating or inhibitory effects in mammalian pLGICs. Although the intersubunit site is an established potentiating site of certain endogenous neurosteroids in the GABA$_A$R, we hypothesize that both sites mediate either potentiation or inhibition for different neurosteroids in pLGICs. Understanding the pharmacology of each respective site will be important for structure-based design of neurosteroid therapeutics. For example, certain neurosteroids may cause potentiation at one site and inhibition at the other at varying concentrations, and such opposing effects may be useful to widen the therapeutic window of novel neurosteroids.

It is interesting to speculate as to the functional significance of these sterol-binding sites in GLIC because bacterial membranes do not contain neurosteroids or other sterols. The equivalent of eukaryotic sterols in bacteria are triterpenoid lipids known as hopanoids, which may have a role in determining the function of prokaryotic pLGICs such as GLIC (53). Furthermore, examination of the GLIC crystal structure shows that both neurosteroid-binding sites identified in this study are occupied by phospholipid densities (34). We hypothesize that these sites are conserved hydrophobic pockets that are occupied by hopanoids in bacterial membranes. These pockets were then assumed by neurosteroids
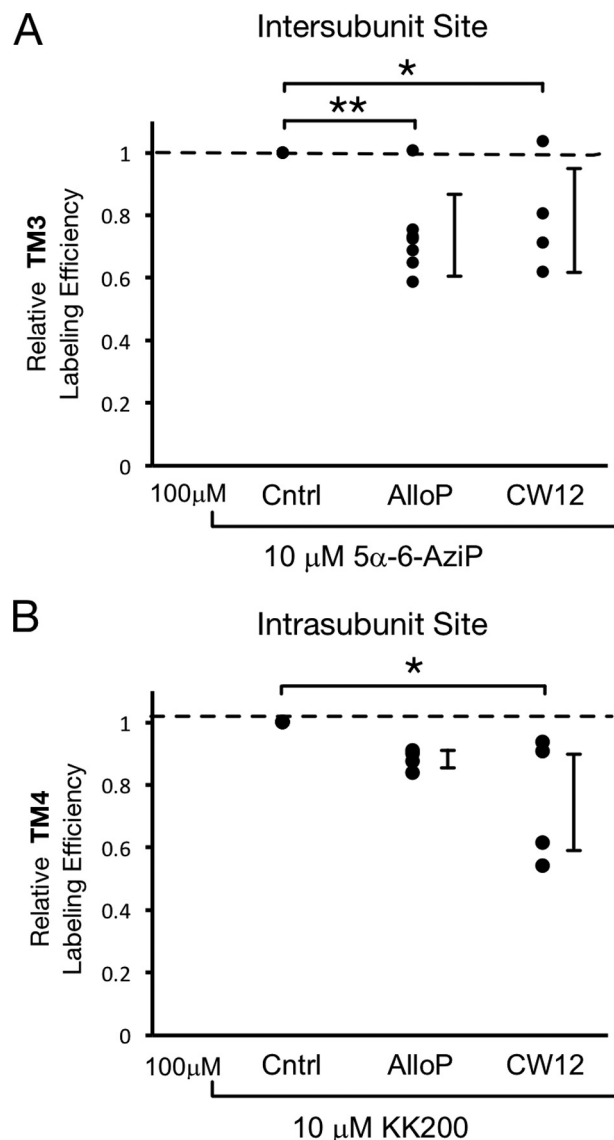

Figure 9. Competitive prevention of neurosteroid labeling at both sites. *A,* photolabeling efficiency of TM3 in WT GLIC by 10 μM 5α-6-AziP in the presence of no competitor (*Cntrl*), 100 μM allopregnanolone (*n* = 7) or CW12 (*n* = 4). Efficiencies are normalized to that of control. ±S.D., *, *p* < 0.05; **, *p* < 0.01. *B,* photolabeling efficiency of TM4 in WT GLIC by 10 μM KK200 in the presence of no competitor (*Cntrl*), 100 μM allopregnanolone (*n* = 4) or CW12 (*n* = 4).

and possibly other sterols in eukaryotic membranes to affect the structural stability and function of mammalian pLGICs. Consistent with this hypothesis, the intrasubunit site identified here was previously noted to satisfy the criteria for a CARC or cholesterol recognition motif, and molecular docking showed that both the hopanoid, diploptene, and cholesterol bind favorably to this site (53).

Experimental procedures

Synthesis of neurosteroid-photolabeling reagents

The syntheses 5α-6-AziP, 5α-12-AziP, 5α-15-AziP, and KK200 are detailed in the supporting Material.

Expression and purification of GLIC

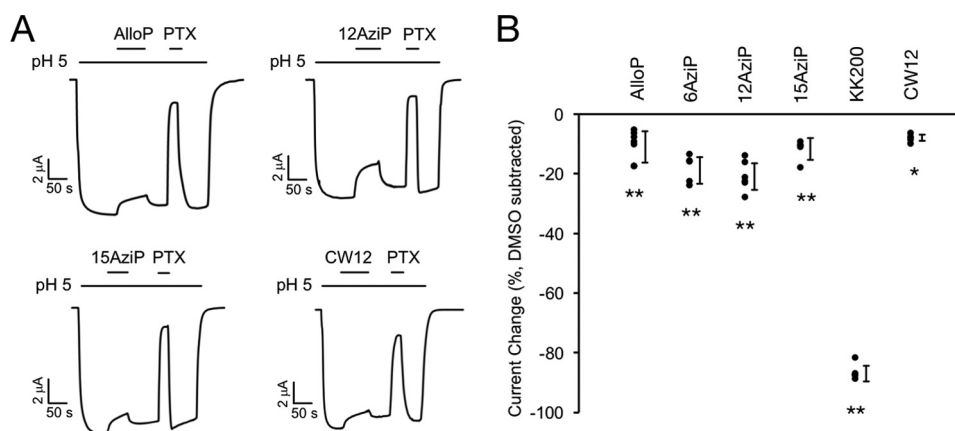pET26-MBP-GLIC was a gift from Raimund Dutzler (Addgene plasmid catalogue no. 20887) and was used for WT GLIC

Figure 10. Neurosteroid inhibition of GLIC WT. *A,* sample current traces from GLIC WT activated by pH 5. 00 (pH$_{50}$) showing the effects of 30 μM allopregnanolone (*AlloP*), 5α-12-AziP (*12AziP*), 5α-15-AziP (*15AziP*), or CW12, and 50 μM picrotoxinin (*PTX*). Traces for 5α-6-AziP (*6AziP*), and KK200 in GLIC WT are shown in Fig. 11. *B,* summary of the functional effects of different neurosteroid analogues on GLIC WT. The effects are shown as DMSO effects subtracted from the effects of steroids in the presence of DMSO. *, $p < 0.05$, and **, $p < 0.001$, for the difference in effect between each neurosteroid analogue and DMSO ($\pm$S.D., *n* at least 5).

Table 1

pH dependence of GLIC WT and mutants

	pH$_{50}$	S.D.	Hill coefficient	S.D.	*n*
WT	4.97	0.12	2.55	0.18	6
I271W	5.48	0.11	1.97	0.29	5
F121A	4.31	0.11	3.45	0.70	6
Y254A	4.19	0.32	1.80	0.63	5

Table 2

Inhibition of GLIC WT and mutants by neurosteroids

	Average % effect	S.E.	*n*	Average DMSO-corrected % effect	S.E.
WT					
Allopregnanolone	−17	2	9	−10	2
5α-6-AziP	−25	2	5	−18	2
5α-12-AziP	−27	2	6	−20	2
5α-15-AziP	−18	2	5	−11	2
KK200	−93	1	5	−86	2
CW12	−15	1	5	−8	1
I271W					
Allopregnanolone	−18	1	6	−8	1
5α-6-AziP	−30	6	5	−20	6
KK200	−17	2	5	−7	2
F121A					
Allopregnanolone	−10	1	8	13	3
5α-6-AziP	14	4	6	37	5
KK200	−23	4	5	0	5
Y254A					
Allopregnanolone	−13	1	9	12	2
5α-6-AziP	−27	2	5	−2	3
KK200	−34	2	4	−9	3

expression. Mutagenesis was performed by oligonucleotide-directed mutagenesis using *Phu* polymerase (Thermo Fisher Scientific) verified by sequencing. GLIC was expressed and purified as described previously (54) in OverExpress™ C43(D3) *Escherichia coli* (Lucigen), derived from BL21(DE3) cells. Briefly, GLIC cultures were grown using Terrific Broth (Sigma) and induced with 0.2 mM isopropyl 1-thio-β-D-galactopyranoside. Cell pellets were reconstituted in Buffer A (50 mM Tris, pH 8, 150 mM NaCl), cOmplete EDTA-free protease inhibitor mixture (Roche Applied Science), and DNase, lysed, and solubilized with 1% DDM. Solubilized protein was purified using Ni-NTA and eluted using Buffer A, 500 mM imidazole, and 0.02% DDM. His-MBP-GLIC was digested overnight with HRV 3c protease (Invitrogen), cleaned up using a reverse Ni-NTA purification, and injected onto a Sephadex 200 Increase

10/300 column, which yielded pentameric GLIC protein in Buffer A + 0.02% DDM.

Photolabeling of GLIC and top-down MS analysis

Purified GLIC was photolabeled and analyzed by top-down MS as described previously (29). For top-down MS analysis, 50 μg of GLIC was mixed with neurosteroid photolabeling reagent at 100, 300, or 100 μM added three times with UV irradiation after each addition. 100-μl samples were irradiated in a quartz cuvette with >320 nm UV light, treated with 250 mM DTT, and then precipitated with chloroform/methanol/water. The precipitated protein was washed three times with equal volumes of water and methanol, centrifuged, and the protein pellet reconstituted in 3 μl of 90% formic acid followed by 50–100 μl of 4:4:1 chloroform/methanol/water. AspN digests were performed by digesting 50 μg of photolabeled GLIC with 2 μg of AspN at room temperature for 15 or 30 h. These digests were then precipitated and reconstituted as described above. Reconstituted samples were then analyzed in an Orbitrap Elite mass spectrometer (Thermo Fisher Scientific) by direct injection at 3 μl/min using a Max Ion API source with a HESI-II probe. Full spectra of photolabeled GLIC were acquired on the linear trap quadrapole using spray voltage of 4 kV, capillary temperature of 320 °C, and in-source dissociation of 30 V. HCD fragmentation spectra were acquired on the Orbitrap at 60,000 resolution, with an AGC target of 5 × 10^5, normalized energy of 10, and 3 *m/z* isolation window. Deconvolution of intact GLIC spectra was performed using MagTran (55). Ion assignments of HCD fragmentation spectra were performed by MASH searching with a mass accuracy of 1.1 Da to account for the "delta 1-Da" error (56); each fragment ion was manually verified and accepted within 10 ppm.

Tryptic middle-down MS analysis

15 μg of photolabeled GLIC was reduced with 5 mM tris(2-carboxyethyl)phosphine for 30 min, alkylated with 5 mM iodoacetamide for 30 min, and quenched with 5 mM DTT. Samples were then digested with 2–6 μg of trypsin for 7 days at 4 °C; extended digestion at low temperature was necessary to obtain maximal recovery of TMD peptides. Next, formic acid was added to 1%, followed directly by LC-MS analysis on an
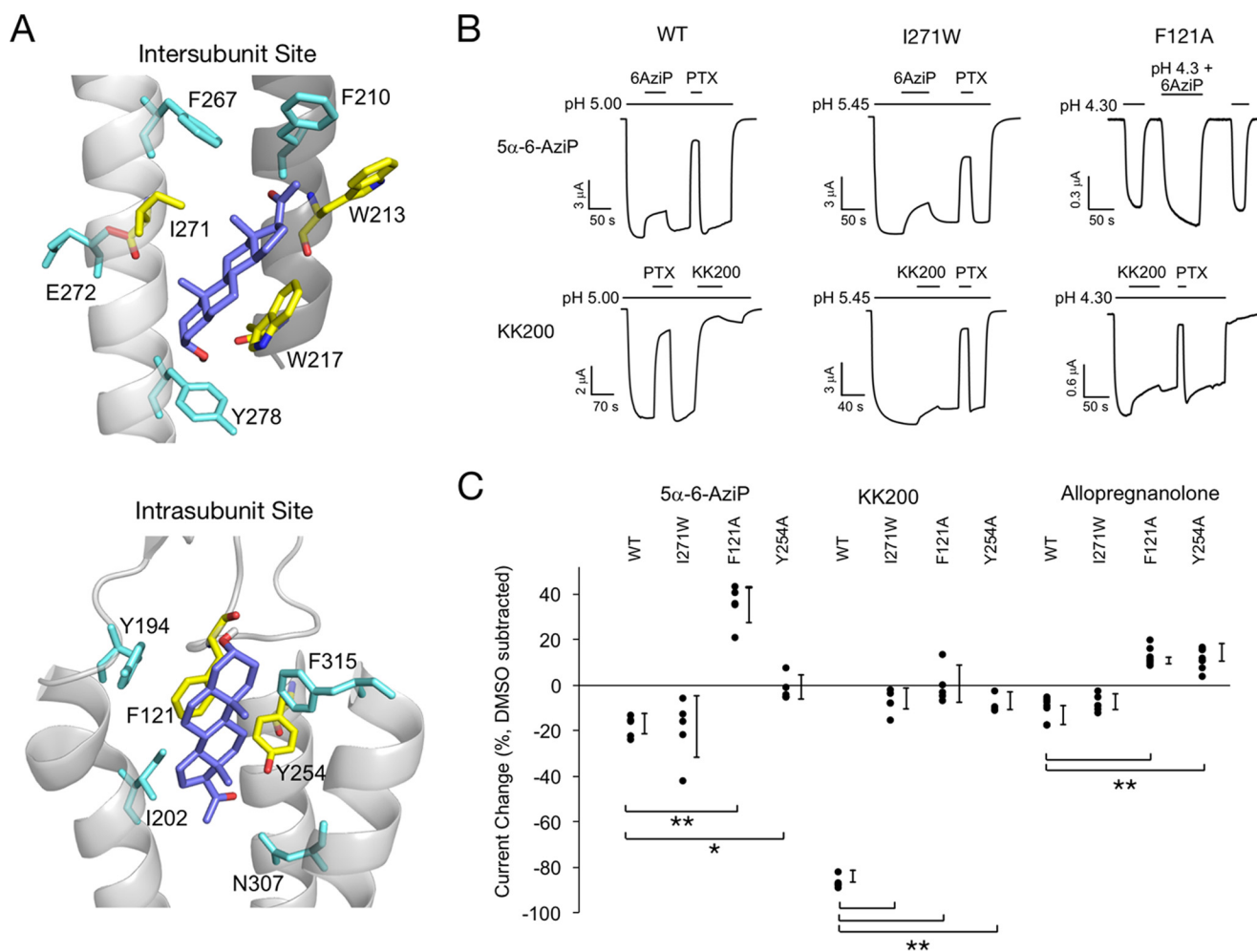
Figure 11. Both neurosteroid-binding sites mediate modulation of GLIC channel activity. *A,* structure of intersubunit and intrasubunit sites highlighting residues that contribute to the allopregnanolone-binding pocket. The preferred allopregnanolone docking pose is shown as *purple sticks*. Residues that were mutated are shown as *yellow sticks*. *B,* sample currents from GLIC WT, I271W, and F121A in the absence and presence of 5α-6-AziP, KK200, and picrotoxinin (*PTX*). *C,* summary of the functional effects of 5α-6-AziP, KK200, and allopregnanolone in WT, I271W, F121A, and Y254A. The effects are shown as DMSO effects subtracted from the effects of steroids in the presence of DMSO (±S.D., *n* at least 5). *, $p < 0.05$; **, $p < 0.001$.

Orbitrap Elite mass spectrometer. 10-µl samples were injected into a home-packed PLRP-S (Agilent) column (10 cm × 75 µm, 300 Å), separated with an 85-min gradient from 10 to 95% acetonitrile, and introduced to the mass spectrometer at 800 nl/min with a nanospray source. MS acquisition was set as an MS1 Orbitrap scan (resolution of 60,000) followed by top 20 MS2 Orbitrap scans (resolution of 15,000) using data-dependent acquisition, 15-s dynamic exclusion, and exclusion of 1+ and 2+ precursors. Fragmentation was performed using CID and HCD with normalized collision energies of 35 and 30, respectively. Analysis of data sets was performed using Xcalibur (Thermo Fisher Scientific) to manually search for TM1 + 2, TM3, or TM4 tryptic peptides with or without neurosteroid photolabel modifications. Photolabeling efficiency was estimated by generating extracted chromatograms of unlabeled and labeled peptides, determining the area under the curve, and calculating the abundance of labeled peptide/(unlabeled + labeled peptide). Competitive inhibition of labeling was performed by labeling GLIC with 10 µM 5α-6-AziP or KK200 in the presence of 100 µM allopregnanolone and CW12. Relative photolabeling efficiency in the absence or presence of competitor was determined for TM3

for 5α-6-AziP and for TM4 for KK200. Analysis of statistical significance comparing the photolabeling efficiency of 5α-6-AziP, 5α-12-AziP, and 5α-15-AziP for GLIC, TM3, and TM1 + 2 or for the competitive inhibition assay was determined using a one-way ANOVA with post hoc corrections using Dunnett's test.

MS2 spectra of photolabeled TMD peptides were analyzed by manual assignment of fragment ions with and without photolabel modification. Fragment ions were accepted based on the presence of a monoisotopic mass within 10 ppm mass accuracy. In addition to manual analysis, PEAKS database searches were performed for data sets of GLIC photolabeled with 5α-6-AziP and KK200 primarily to search for photolabeled ECD tryptic peptides. Search parameters were set for a precursor mass accuracy of 10 ppm, fragment ion accuracy of 0.1 Da, up to three missed cleavages on either end of the peptide, and variable modifications of methionine oxidation, cysteine carbamidomethylation, and 5α-6-AziP or KK200 on any amino acid.

Electrophysiology experiments

The cDNAs for oocyte expression were subcloned into the pcDNA3 vector with the modification that the maltose-binding

protein was replaced with the signal peptide of the human $\beta 3$ GABA-A subunit. The T7 promoter was used for RNA synthesis and linearized by XbaI (New England Biolabs). The cRNAs were produced using mMessage mMachine (Ambion). Oocytes were injected with 5 ng of cRNA and incubated for 1–3 days prior to recording. The electrophysiological experiments were conducted using a standard two-electrode voltage clamp. Voltage and current electrodes were borosilicate patch-clamp electrodes (G120F-4, outer diameter = 1.20 mm, inner diameter = 0.69 mm, Warner Instruments, Hamden, CT) that were filled with 3 M KCl and had resistance of less than 1 megohm. The oocytes were clamped at −60 mV. Solutions were gravity-applied from 30-ml glass syringes via Teflon tubing to reduce adsorption. Oocytes were perfused continuously with ND96 (96 mM NaCl, 2 mM KCl, 1 mM MgCl$_2$, 1.8 mM CaCl$_2$, 5 mM HEPES) solution at pH 7.6 at ~5 ml/min. Proton-elicited currents were measured by exposing the cells to ND96 buffered at pH 7.0 to 3.5. At lower pH values, HEPES was replaced with 5 mM MES (pH 6–5.45) or 5 mM sodium citrate (pH 5.0–3.5). Solutions were switched manually.

The pH-response relationships were determined by exposing an oocyte to 4–7 different pH solutions. The concentration-response data were fit to Equation 1,

$$ I = \frac{I_{max}}{1 + 10^{(pH - pH_{50}) \times n_H}} \tag{Eq. 1} $$

where I is the peak response to a given pH; I_{max} is the maximal fitted amplitude; pH_{50} is the pH eliciting half-maximal response; and n_H is the Hill coefficient.

The effects of steroid on the function of GLIC were studied at pH_{50}. Each oocyte was additionally exposed to picrotoxinin (in pH_{50}), a known blocker of GLIC (57), to exclude any drastic effects of mutations on receptor function that may have masked the effects on modulation by steroids. Exposure to 50 μM picrotoxinin reduced the pH_{50} current levels to 19 ± 1% of control in WT and 30 ± 3% ($p < 0.05$ *versus* wildtype; ANOVA with Dunnett's post hoc correction), 13 ± 1% ($p > 0.55$), or 26 ± 5% ($p > 0.23$) of control in I271W, F121A, and Y254A, respectively.

A typical experiment (Fig. 4B) consisted of recording of a 10–20-s baseline at pH 7.6, followed by exposure to pH_{50} until a steady response was obtained. The receptor was then exposed to 30 μM steroid in pH_{50} (maximal application duration 65 s), followed by recovery in the pH_{50} solution and an application of 50 μM picrotoxinin. WT GLIC exposed to KK200 exhibited strong block and slow washout; accordingly, the effect of picrotoxinin was tested before steroid application (Fig. 4B). The F121A mutant exhibited unstable transient responses upon switch from pH_{50} to pH_{50} + 5α-6-AziP. For this combination, the effect of steroid was determined by comparing peak responses to applications of pH_{50} or pH_{50} + 5α-6-AziP, separated by a brief wash in pH 7.6 solution (Fig. 4B).

The concentration of DMSO in final steroid solutions was 0.3% (v/v). In control experiments we tested the effect of 0.3% DMSO on GLIC function. Oocytes expressing wildtype or mutant receptors activated by pH_{50} showed inhibition in the presence of DMSO. The average inhibitory effect was 7 ± 1, 10 ± 1, 23 ± 3, or 25 ± 2% (n = 5 cells for each) for wildtype, I271W,

F121A, and Y254A, respectively. The data for steroid effects are reported after subtraction of the DMSO-only effect.

Current responses were amplified with an OC-725C amplifier (Warner Instruments), filtered at 40 Hz, digitized with a Digidata 1200 series digitizer (Molecular Devices) at a 100 Hz sampling rate, and stored using pClamp (Molecular Devices). The traces were subsequently analyzed with Clampfit (Molecular Devices) to determine the maximal amplitude of current response.

GLIC was expressed in oocytes from the African clawed frog (*Xenopus laevis*). Frogs were purchased from *Xenopus* 1 (Dexter, MI) and housed and cared for in a Washington University Animal Care Facility under the supervision of the Washington University Division of Comparative Medicine. Harvesting of oocytes was conducted in accordance with the Guide for the Care and Use of Laboratory Animals as adopted and promulgated by the National Institutes of Health. The protocol is approved by the Animal Studies Committee of Washington University in St. Louis (Approval No. 20170071).

Docking simulations

Docking was performed using AutoDock 4.2 (58). The GLIC template was prepared using PDB 4FHI in AutoDock Tools by deleting waters, adding hydrogens, computing Gasteiger charges, and merging non-polar hydrogens. Allopregnanolone was prepared by converting the sdf file from PubChem into a PDB file using Open Babel (48), and Gasteiger charges and free torsion angles were determined by AutoDock Tools. Structures for 5α-12-AziP, 5α-15-AziP, CW12, and KK200 were obtained by modifying the allopregnanolone in Maestro (Academic version, Schrodinger) using the 2D draw and 3D conversion function, after which Gasteiger charges and free torsion angles were determined by AutoDock Tools. Four docking simulations were performed for allopregnanolone using templates of 1) the entire TMD of two adjacent GLIC subunits (50 × 42 × 50 Å); 2) the entire TMD of two adjacent GLIC subunits (50 × 42 × 50 Å) with one allopregnanolone molecule within the intersubunit site (Note: this was necessary to adequately sample binding modes outside of the intersubunit site.); 3) the intersubunit site (36 × 32 × 34 Å); and 4) the intrasubunit site (32 × 30 × 32 Å). The photolabeling reagents were docked to grid boxes encompassing only the intersubunit and intrasubunit sites. All simulations were performed with 1-Å grid spacing, using a genetic algorithm with 250 runs, and otherwise default parameters. Results were clustered using a 2-Å root mean square deviation. For each neurosteroid photolabeling ligand, the three most populated clusters were examined, and shown are poses where the photolabeling moiety is in closest proximity to the labeled residue.

Neurosteroid-binding sites in GLIC

References

1. Lambert, J. J., Belelli, D., Hill-Venning, C., and Peters, J. A. (1995) Neurosteroids and GABA$_A$ receptor function. *Trends Pharmacol. Sci.* **16,** 295–303 CrossRef Medline

2. Bertrand, D., Valera, S., Bertrand, S., Ballivet, M., and Rungger, D. (1991) Steroids inhibit nicotinic acetylcholine receptors. *Neuroreport* **2,** 277–280 CrossRef Medline

3. Gillo, B., and Lass, Y. (1984) The mechanism of steroid anaesthetic (alphaxalone) block of acetylcholine-induced ionic currents. *Br. J. Pharmacol.* **82,** 783–789 CrossRef Medline

4. Maksay, G., Laube, B., and Betz, H. (2001) Subunit-specific modulation of glycine receptors by neurosteroids. *Neuropharmacology* **41,** 369–376 CrossRef Medline

5. Jiang, P., Yang, C. X., Wang, Y. T., and Xu, T. L. (2006) Mechanisms of modulation of pregnanolone on glycinergic response in cultured spinal dorsal horn neurons of rat. *Neuroscience* **141,** 2041–2050 CrossRef Medline

6. Belelli, D., and Lambert, J. J. (2005) Neurosteroids: endogenous regulators of the GABA(A) receptor. *Nat. Rev. Neurosci.* **6,** 565–575 CrossRef Medline

7. Reddy, D. S., and Estes, W. A. (2016) Clinical potential of neurosteroids for CNS disorders. *Trends Pharmacol. Sci.* **37,** 543–561 CrossRef Medline

8. Harrison, N. L., and Simmonds, M. A. (1984) Modulation of the GABA receptor complex by a steroid anaesthetic. *Brain Res.* **323,** 287–292 CrossRef Medline

9. Deleted in proof

10. Zorumski, C. F., Paul, S. M., Izumi, Y., Covey, D. F., and Mennerick, S. (2013) Neurosteroids, stress and depression: potential therapeutic opportunities. *Neurosci. Biobehav. Rev.* **37,** 109–122 CrossRef Medline

11. Vallée, M. (2016) Neurosteroids and potential therapeutics: focus on pregnenolone. *J. Steroid Biochem. Mol. Biol.* **160,** 78–87 CrossRef Medline

12. Shu, H. J., Eisenman, L. N., Jinadasa, D., Covey, D. F., Zorumski, C. F., and Mennerick, S. (2004) Slow actions of neuroactive steroids at GABAA receptors. *J. Neurosci.* **24,** 6667–6675 CrossRef Medline

13. Park-Chung, M., Malayev, A., Purdy, R. H., Gibbs, T. T., and Farb, D. H. (1999) Sulfated and unsulfated steroids modulate γ-aminobutyric acid A receptor function through distinct sites. *Brain Res.* **830,** 72–87 CrossRef Medline

14. Wang, M., He, Y., Eisenman, L. N., Fields, C., Zeng, C. M., Mathews, J., Benz, A., Fu, T., Zorumski, E., Steinbach, J. H., Covey, D. F., Zorumski, C. F., and Mennerick, S. (2002) 3β-Hydroxypregnane steroids are pregnenolone sulfate-like GABA(A) receptor antagonists. *J. Neurosci.* **22,** 3366–3375 Medline

15. Li, P., Covey, D. F., Steinbach, J. H., and Akk, G. (2006) Dual potentiating and inhibitory actions of a benz[*e*]indene neurosteroid analog on recombinant α1β2γ2 GABAA receptors. *Mol. Pharmacol.* **69,** 2015–2026 CrossRef Medline

16. Paradiso, K., Sabey, K., Evers, A. S., Zorumski, C. F., Covey, D. F., and Steinbach, J. H. (2000) Steroid inhibition of rat neuronal nicotinic α4β2 receptors expressed in HEK 293 cells. *Mol. Pharmacol.* **58,** 341–351 CrossRef Medline

17. Mensah-Nyagan, A. G., Meyer, L., Schaeffer, V., Kibaly, C., and Patte-Mensah, C. (2009) Evidence for a key role of steroids in the modulation of pain. *Psychoneuroendocrinology* **34,** S169–S177 CrossRef Medline

18. Akk, G., Shu, H. J., Wang, C., Steinbach, J. H., Zorumski, C. F., Covey, D. F., and Mennerick, S. (2005) Neurosteroid access to the GABAA receptor. *J. Neurosci.* **25,** 11605–11613 CrossRef Medline

19. Chisari, M., Eisenman, L. N., Krishnan, K., Bandyopadhyaya, A. K., Wang, C., Taylor, A., Benz, A., Covey, D. F., Zorumski, C. F., and Mennerick, S. (2009) The influence of neuroactive steroid lipophilicity on GABAA receptor modulation: evidence for a low-affinity interaction. *J. Neurophysiol.* **102,** 1254–1264 CrossRef Medline

20. Covey, D. F., Nathan, D., Kalkbrenner, M., Nilsson, K. R., Hu, Y., Zorumski, C. F., and Evers, A. S. (2000) Enantioselectivity of pregnanolone-induced γ-aminobutyric acid(A) receptor modulation and anesthesia. *J. Pharmacol. Exp. Ther.* **293,** 1009–1016 Medline

21. Chen, Z. W., Manion, B., Townsend, R. R., Reichert, D. E., Covey, D. F., Steinbach, J. H., Sieghart, W., Fuchs, K., and Evers, A. S. (2012) Neurosteroid analog photolabeling of a site in the third transmembrane domain of the β3 subunit of the GABA(A) receptor. *Mol. Pharmacol.* **82,** 408–419 CrossRef Medline

22. Laverty, D., Thomas, P., Field, M., Andersen, O. J., Gold, M. G., Biggin, P. C., Gielen, M., and Smart, T. G. (2017) Crystal structures of a GABAA-receptor chimera reveal new endogenous neurosteroid-binding sites. *Nat. Struct. Mol. Biol.* **24,** 977–985 CrossRef Medline

23. Miller, P. S., Scott, S., Masiulis, S., De Colibus, L., Pardon, E., Steyaert, J., and Aricescu, A. R. (2017) Structural basis for GABAA receptor potentiation by neurosteroids. *Nat. Struct. Mol. Biol.* **24,** 986–992 CrossRef Medline

24. Akk, G., Bracamontes, J. R., Covey, D. F., Evers, A., Dao, T., and Steinbach, J. H. (2004) Neuroactive steroids have multiple actions to potentiate GABAA receptors. *J. Physiol.* **558,** 59–74 CrossRef Medline

25. Hosie, A. M., Wilkins, M. E., da Silva, H. M., and Smart, T. G. (2006) Endogenous neurosteroids regulate GABAA receptors through two discrete transmembrane sites. *Nature* **444,** 486–489 CrossRef Medline

26. Evers, A. S., Chen, Z. W., Manion, B. D., Han, M., Jiang, X., Darbandi-Tonkabon, R., Kable, T., Bracamontes, J., Zorumski, C. F., Mennerick, S., Steinbach, J. H., and Covey, D. F. (2010) A synthetic 18-norsteroid distinguishes between two neuroactive steroid binding sites on GABAA receptors. *J. Pharmacol. Exp. Ther.* **333,** 404–413 CrossRef Medline

27. Woll, K. A., Dailey, W. P., Brannigan, G., and Eckenhoff, R. G. (2016) Shedding light on anesthetic mechanisms: application of photoaffinity ligands. *Anesth. Analg.* **123,** 1253–1262 CrossRef Medline

28. Das, J. (2011) Aliphatic diazirines as photoaffinity probes for proteins: recent developments. *Chem. Rev.* **111,** 4405–4417 CrossRef Medline

29. Budelier, M. M., Cheng, W. W., Bergdoll, L., Chen, Z. W., Janetka, J. W., Abramson, J., Krishnan, K., Mydock-McGrane, L., Covey, D. F., Whitelegge, J. P., and Evers, A. S. (2017) Photoaffinity labeling with cholesterol analogues precisely maps a cholesterol-binding site in voltage-dependent anion channel-1. *J. Biol. Chem.* **292,** 9294–9304 CrossRef Medline

30. Budelier, M. M., Cheng, W. W., Bergdoll, L., Chen, Z. W., Abramson, J., Krishnan, K., Qian, M., Covey, D. F., Janetka, J. W., and Evers, A. S. (2017) Click chemistry reagent for identification of sites of covalent ligand incorporation in integral membrane proteins. *Anal. Chem.* **89,** 2636–2644 CrossRef Medline

31. Savechenkov, P. Y., Chiara, D. C., Desai, R., Stern, A. T., Zhou, X., Ziemba, A. M., Szabo, A. L., Zhang, Y., Cohen, J. B., Forman, S. A., Miller, K. W., and Bruzik, K. S. (2017) Synthesis and pharmacological evaluation of neurosteroid photoaffinity ligands. *Eur. J. Med. Chem.* **136,** 334–347 CrossRef Medline

32. Darbandi-Tonkabon, R., Hastings, W. R., Zeng, C. M., Akk, G., Manion, B. D., Bracamontes, J. R., Steinbach, J. H., Mennerick, S. J., Covey, D. F., and Evers, A. S. (2003) Photoaffinity labeling with a neuroactive steroid analogue. 6-Azi-pregnanolone labels voltage-dependent anion channel-1 in rat brain. *J. Biol. Chem.* **278,** 13196–13206 CrossRef Medline

33. Chen, Z. W., Wang, C., Krishnan, K., Manion, B. D., Hastings, R., Bracamontes, J., Taylor, A., Eaton, M. M., Zorumski, C. F., Steinbach, J. H., Akk, G., Mennerick, S., Covey, D. F., and Evers, A. S. (2014) 11-Trifluoromethyl-phenyldiazirinyl neurosteroid analogues: potent general anesthetics and photolabeling reagents for GABAA receptors. *Psychopharmacology* **231,** 3479–3491 CrossRef Medline

34. Bocquet, N., Nury, H., Baaden, M., Le Poupon, C., Changeux, J. P., Delarue, M., and Corringer, P. J. (2009) X-ray structure of a pentameric ligand-gated ion channel in an apparently open conformation. *Nature* **457,** 111–114 CrossRef Medline

35. daCosta, C. J., and Baenziger, J. E. (2013) Gating of pentameric ligand-gated ion channels: structural insights and ambiguities. *Structure* **21,** 1271–1283 CrossRef Medline

36. Pan, J., Chen, Q., Willenbring, D., Mowrey, D., Kong, X. P., Cohen, A., Divito, C. B., Xu, Y., and Tang, P. (2012) Structure of the pentameric ligand-gated ion channel GLIC bound with anesthetic ketamine. *Structure* **20,** 1463–1469 CrossRef Medline

SASBMB

37. Nury, H., Van Renterghem, C., Weng, Y., Tran, A., Baaden, M., Dufresne, V., Changeux, J. P., Sonner, J. M., Delarue, M., and Corringer, P. J. (2011) X-ray structures of general anaesthetics bound to a pentameric ligand-gated ion channel. *Nature* **469,** 428–431 CrossRef Medline

38. Fourati, Z., Ruza, R. R., Laverty, D., Drège, E., Delarue-Cochin, S., Joseph, D., Koehl, P., Smart, T., and Delarue, M. (2017) Barbiturates bind in the GLIC ion channel pore and cause inhibition by stabilizing a closed state. *J. Biol. Chem.* **292,** 1550–1558 CrossRef Medline

39. Murail, S., Howard, R. J., Broemstrup, T., Bertaccini, E. J., Harris, R. A., Trudell, J. R., and Lindahl, E. (2012) Molecular mechanism for the dual alcohol modulation of Cys-loop receptors. *PLoS Comput. Biol.* **8,** e1002710 CrossRef Medline

40. Howard, R. J., Murail, S., Ondricek, K. E., Corringer, P. J., Lindahl, E., Trudell, J. R., and Harris, R. A. (2011) Structural basis for alcohol modulation of a pentameric ligand-gated ion channel. *Proc. Natl. Acad. Sci. U.S.A.* **108,** 12149–12154 CrossRef Medline

41. Chen, Q., Cheng, M. H., Xu, Y., and Tang, P. (2010) Anesthetic binding in a pentameric ligand-gated ion channel: GLIC. *Biophys J* **99,** 1801–1809 CrossRef Medline

42. Laurent, B., Murail, S., Shahsavar, A., Sauguet, L., Delarue, M., and Baaden, M. (2016) Sites of anesthetic inhibitory action on a cationic ligand-gated ion channel. *Structure* **24,** 595–605 CrossRef Medline

43. Chiara, D. C., Gill, J. F., Chen, Q., Tillman, T., Dailey, W. P., Eckenhoff, R. G., Xu, Y., Tang, P., and Cohen, J. B. (2014) Photoaffinity labeling the propofol binding site in GLIC. *Biochemistry* **53,** 135–142 CrossRef Medline

44. Giansanti, P., Tsiatsiani, L., Low, T. Y., and Heck, A. J. (2016) Six alternative proteases for mass spectrometry-based proteomics beyond trypsin. *Nat. Protoc.* **11,** 993–1006 CrossRef Medline

45. Sauguet, L., Poitevin, F., Murail, S., Van Renterghem, C., Moraga-Cid, G., Malherbe, L., Thompson, A. W., Koehl, P., Corringer, P. J., Baaden, M., and Delarue, M. (2013) Structural basis for ion permeation mechanism in pentameric ligand-gated ion channels. *EMBO J.* **32,** 728–741 CrossRef Medline

46. Harrison, N. L., Majewska, M. D., Harrington, J. W., and Barker, J. L. (1987) Structure-activity relationships for steroid interaction with the γ-aminobutyric acid A receptor complex. *J. Pharmacol. Exp. Ther.* **241,** 346–353 Medline

47. Li, W., Jin, X., Covey, D. F., and Steinbach, J. H. (2007) Neuroactive steroids and human recombinant ρ1 GABAC receptors. *J. Pharmacol. Exp. Ther.* **323,** 236–247 CrossRef Medline

48. O'Boyle, N. M., Banck, M., James, C. A., Morley, C., Vandermeersch, T., and Hutchison, G. R. (2011) Open babel: an open chemical toolbox. *J. Cheminform.* **3,** 33 CrossRef Medline

49. Brunner, J. (1993) New photolabeling and crosslinking methods. *Annu. Rev. Biochem.* **62,** 483–514 CrossRef Medline

50. Akk, G., Covey, D. F., Evers, A. S., Mennerick, S., Zorumski, C. F., and Steinbach, J. H. (2010) Kinetic and structural determinants for GABA-A receptor potentiation by neuroactive steroids. *Curr. Neuropharmacol.* **8,** 18–25 CrossRef Medline

51. Paradiso, K., Zhang, J., and Steinbach, J. H. (2001) The C terminus of the human nicotinic α4β2 receptor forms a binding site required for potentiation by an estrogenic steroid. *J. Neurosci.* **21,** 6561–6568 Medline

52. Ghosh, B., Tsao, T. W., and Czajkowski, C. (2017) A chimeric prokaryotic-eukaryotic pentameric ligand-gated ion channel reveals interactions between the extracellular and transmembrane domains shape neurosteroid modulation. *Neuropharmacology* **125,** 343–352 CrossRef Medline

53. Barrantes, F. J., and Fantini, J. (2016) From hopanoids to cholesterol: Molecular clocks of pentameric ligand-gated ion channels. *Prog. Lipid Res.* **63,** 1–13 CrossRef Medline

54. Hilf, R. J., and Dutzler, R. (2009) Structure of a potentially open state of a proton-activated pentameric ligand-gated ion channel. *Nature* **457,** 115–118 CrossRef Medline

55. Zhang, Z., and Marshall, A. G. (1998) A universal algorithm for fast and automated charge state deconvolution of electrospray mass-to-charge ratio spectra. *J. Am. Soc. Mass Spectrom.* **9,** 225–233 CrossRef Medline

56. Guner, H., Close, P. L., Cai, W., Zhang, H., Peng, Y., Gregorich, Z. R., and Ge, Y. (2014) MASH Suite: a user-friendly and versatile software interface for high-resolution mass spectrometry data interpretation and visualization. *J. Am. Soc. Mass Spectrom.* **25,** 464–470 CrossRef Medline

57. Alqazzaz, M., Thompson, A. J., Price, K. L., Breitinger, H. G., and Lummis, S. C. (2011) Cys-loop receptor channel blockers also block GLIC. *Biophys. J.* **101,** 2912–2918 CrossRef Medline

58. Morris, G. M., Huey, R., Lindstrom, W., Sanner, M. F., Belew, R. K., Goodsell, D. S., and Olson, A. J. (2009) AutoDock4 and AutoDockTools4: Automated docking with selective receptor flexibility. *J. Comput. Chem.* **30,** 2785–2791 CrossRef Medline

Mapping two neurosteroid-modulatory sites in the prototypic pentameric ligand-gated ion channel GLIC

Wayland W. L. Cheng, Zi-Wei Chen, John R. Bracamontes, Melissa M. Budelier,
Kathiresan Krishnan, Daniel J. Shin, Cunde Wang, Xin Jiang, Douglas F. Covey,
Gustav Akk and Alex S. Evers